Journal of Solid State Chemistry 183 (2010) 173–179

Contents lists available at ScienceDirect

Journal of Solid State Chemistry

journal homepage: www.elsevier.com/locate/jssc

Crystal structures of three intermetallic phases in the Mo–Pt–Si system

J.-M. Joubert [a,*], Ya. Tokaychuk [a,1], R. Černý [b]

[a] Chimie Métallurgique des Terres Rares, Institut de Chimie et des Matériaux Paris-Est, CNRS, Université de Paris XII, UMR 7182, 2-8 rue Henri Dunant, F-94320 Thiais, France
[b] Laboratoire de Cristallographie, Université de Genève, Quai E. Ansermet, CH-1211 Genève 4, Switzerland

ARTICLE INFO

Article history:
Received 10 August 2009
Received in revised form
27 October 2009
Accepted 1 November 2009
Available online 10 November 2009

Keywords:
Mo–Pt–Si
Intermetallic compound
Ab initio powder structure determination
Silicide
Frank-Kasper

ABSTRACT

The crystal structures of three ternary Mo–Pt–Si intermetallic compounds have been determined *ab initio* from powder X-ray diffraction data. All three structures are representative of new structure types. Both the *X* ($MoPt_2Si_3$, $Pmc2_1$, *oP*12, a=3.48438(6), b=9.1511(2), c=5.48253(8) Å) and *Y* ($MoPt_3Si_4$, *Pnma*, *oP*32, a=5.51210(9), b=3.49474(7), c=24.3090(4) Å) phases derive from PtSi (FeAs type) structure while the *Z* phase (ideal composition $Mo_{32}Pt_{20}Si_{16}$, refined composition $Mo_{29.9(2)}Pt_{21.0(3)}Si_{17.1(1)}$, *Cc*, *mC*68, a=13.8868(3), b=8.0769(2), c=9.6110(2) Å, β=100.898(1)°) present similarities with the group of Frank-Kasper phases.

1. Introduction

The outstanding high temperature oxidation resistance of $MoSi_2$ [1] has motivated the study of ternary systems of refractory transition elements with silicon which are of high interest for high temperature applications. The study of the ternary phase diagram of the Mo–Pt–Si ternary system has evidenced the presence of three ternary intermetallic phases with approximate compositions $MoPt_2Si_3$ (*X*), $MoPt_3Si_4$ (*Y*) and $Mo_3Pt_2Si_2$ (*Z*) [2–4]. The structure of these compounds has remained essentially undetermined. Only the cell parameters of the *Y* phase was known [2]. The purpose of the present work is to perform a complete structure determination of the three phases. This was achieved *ab initio* by the analysis of powder diffraction data.

2. Experimental details

2.1. Synthesis and characterization

The stoichiometric amounts of metal powders (Mo: 99.9%, −250 mesh, Alfa Aesar; Pt: 99.9%, < 60 μm, Chempur; Si: 99.999%, Cerac) were mixed in a mortar and pressed into pellets. After outgassing under high vacuum, these pellets were melted in an arc furnace on a water-cooled copper hearth under argon atmosphere. To ensure homogeneity, each sample was re-melted four times. No significant weight loss was observed. An annealing treatment was performed in a silica tube under high vacuum after wrapping the samples in a tantalum foil to avoid the direct contact with silica. The temperatures (see Table 1) were chosen to conform the isothermal sections of Mo–Pt–Si system determined in previous work [3,4] (*X* and *Y* are stable at 1150°, *Z* decomposes between 1020 and 1150 °C). The silica tubes were subsequently quenched into cold water. Small pieces of the samples were polished and their microstructure was analysed by electronic metallography. The number of phases and their composition were obtained by electron probe micro-analysis (EPMA, CAMECA SX100).

2.2. Data acquisition

The powder X-ray diffraction data for the two phases *X* and *Y* were collected at room temperature on a Bruker D8-Advance diffractometer equipped with a graphite monochromator installed in the diffracted beam (Bragg-Brentano, Cu*K*α-radiation, sample diameter 20 mm, for other details see Table 2). The structure of the *Z* phase was too complex to be solved from laboratory data. For this phase, the data were collected on the powder diffractometer of the Swiss Norwegian Beamline installed at the ESRF (Grenoble, France). This diffractometer works in the Debye–Scherrer geometry with a multi-stage analyser in the diffracted beam. The sample was filled in a capillary of diameter $2R$=0.3 mm to maximize the diffraction signal keeping the absorption factor $p.\mu.R$ (where p is the packing of the powder

* Corresponding author. Fax: +33 1 49 78 12 03.
E-mail address: jean-marc.joubert@icmpe.cnrs.fr (J.-M. Joubert).
[1] Present address: Department of Inorganic Chemistry, Ivan Franko National University of Lviv, Kyryla i Mefodiya Str., 6, 79005 Lviv, Ukraine.

0022-4596/$ - see front matter © 2009 Elsevier Inc. All rights reserved.
doi:10.1016/j.jssc.2009.11.006

and μ the linear absorption factor) close to one, at the chosen wavelength (see Table 2) which was refined with a Si standard.

2.3. Indexing and structure solution

When the cell was unknown, the indexing was performed with the programs Dicvol 91 [5] and Topas [6]. The possible space groups were derived from the examination of the extinctions. The mass density of the ternary compounds was estimated from the known densities of the binary ones in Mo–Pt, Pt–Si and Mo–Si systems. Together with the measured composition of each phase, it allows to determine the approximate number of atoms of each type in the unit cell. The structure solution was found in the direct space by global optimization of the parameters using the program FOX [7].

Table 1
Synthesis and characterization of the samples.

Nominal composition	Heat treatment (time (days), temperature (°C))	Present phases (X-ray)	Phase composition (EPMA) (at%)
$Mo_{16.7}Pt_{33.3}Si_{50}$ ($MoPt_2Si_3$)	30, 1150	*X*	$Mo_{17.1(1)}Pt_{33.2(1)}Si_{49.7(1)}$
		$MoSi_2$	
$Mo_{12.5}Pt_{37.5}Si_{50}$ ($MoPt_3Si_4$)	21, 1150	*Y*	$Mo_{12.7(1)}Pt_{37.3(1)}Si_{50.0(1)}$
		Mo_5Si_3	Not detected
		PtSi	$Pt_{51.0(4)}Si_{49.0(3)}Mo_{0.0(1)}$
		Pt_2Si	$Pt_{66.0(6)}Si_{33.4(4)}Mo_{0.6(5)}$
$Mo_{42.9}Pt_{28.6}Si_{28.6}$ ($Mo_3Pt_2Si_2$)	36, 1020	*Z*	$Mo_{42.5(1)}Pt_{29.6(1)}Si_{27.9(1)}$
		Mo_5Si_3	Not detected
		Other phase	Not detected

2.4. Structure refinement

The structural model obtained at the previous step was refined using the Rietveld method with the program Fullprof [8]. The anomalous scattering parameters at the wavelength of the measurement were taken into account for the refinement of the *Z* phase, as well as the correction for polarization and absorption as usual for synchrotron measurements. When necessary, a correction for preferential orientation, anisotropic line broadening or sites with mixed occupancies were introduced. Low and even negative refined atomic displacement parameters for Bragg–Brentano data (*X* and *Y* phases) are observed and are related to the phenomenon of micro-absorption caused by the extremely large linear absorption coefficient of the compounds at the Cu*K*α wavelength. A correction for the micro-absorption has not been introduced since its effect on the diffracted intensities is almost undistinguishable from that of the displacement parameters and it cannot be refined independently. We preferred therefore to refine only the displacement parameters, being aware that their value is not significant. It will not be given.

3. Results

3.1. Characterization

The results of the characterization of the three samples are presented in Table 1. Besides the new ternary compounds *X* and *Y* of analyzed compositions very close to $MoPt_2Si_3$ and $MoPt_3Si_4$, the samples of nominal compositions $Mo_{16.7}Pt_{33.3}Si_{50}$ and $Mo_{12.5}Pt_{37.5}Si_{50}$ contained small quantities of the binary phases $MoSi_2$, PtSi or Pt_2Si. No additional phase could be detected with EPMA in the sample of nominal composition $Mo_{42.9}Pt_{28.6}Si_{28.6}$.

3.2. X phase

In the pattern of the sample $Mo_{16.7}Pt_{33.3}Si_{50}$, 19 strong independent peaks of the *X* phase were indexed in an orthor-

Table 2
Data collection and structure refinement details for the three studied compounds.

Compound	*X*–$MoPt_2Si_3$	*Y*–$MoPt_3Si_4$	*Z*
Sample composition (in at%)	$Mo_{16.7}Pt_{33.3}Si_{50}$	$Mo_{12.5}Pt_{37.5}Si_{50}$	$Mo_{42.9}Pt_{28.6}Si_{28.6}$
Phase composition (in at%)	$Mo_{17.1(1)}Pt_{33.2(1)}Si_{49.7(1)}$	$Mo_{12.7(1)}Pt_{37.3(1)}Si_{50.0(1)}$	$Mo_{42.5(1)}Pt_{29.6(1)}Si_{27.9(1)}$
Abundance, wt%	95.3(5)	95.1(5)	92(1)
Diffractometer; λ (Å)	Bruker D8; Cu$K\alpha_{1,2}$	Bruker D8; K$\alpha_{1,2}$	Synchrotron; 0.40047(1)
$2\theta_{min-max}$ (deg)	15–140	14–140	1.025–45.460
Step size, deg; profile points	0.04; 3125	0.04; 3150	0.0025; 17774
Number of "independent" and "effective" reflections (see Fullprof manual)	261; 175	857; 293	4717; 592
Number of refined structural parameters	16	21	59
Space group	$Pmc2_1$	*Pnma*	*Cc*
Pearson code, *Z*	*oP*12	*oP*32	*mC*68
Cell parameters			
a (Å)	3.48438(6)	5.51210(9)	13.8868(3)
b (Å)	9.1511(2)	3.49474(7)	8.0769(2)
c (Å)	5.48253(9)	24.3090(4)	9.6110(2)
β (deg)			100.898(1)
Cell volume *V* (Å^3)	174.816(5)	468.27(2)	1058.54(4)
Preferred orientation: direction, value	[010]; 0.913(2)	[112]; 1.131(4)	
Reliability factors			
R_B (%)	3.84	4.39	6.22
R_F (%)	2.23	3.38	4.32
R_p[a] (%)	7.08; 5.59	8.77; 5.33	12.2; 5.96
R_{wp}[a] (%)	8.66; 7.08	10.02; 6.84	13.2; 7.60
χ^2	13.0	3.92	2.43

[a] Conventional and non-corrected for background.

hombic unit cell with parameters: a=5.4866, b=3.4870, c=9.1597 Å. The analysis of the systematic extinctions of the Bragg reflections led to the possible space groups *Pmma*, *Pm*2*a* and $P2_1ma$. The positions of the heavy atoms (Pt and Mo) were successfully determined using FOX in the centrosymmetric space group *Pmma*. However, problems occurred when finding the Si positions that were solved by lowering the symmetry to $P2_1ma$ (non-standard setting of $Pmc2_1$). Structure solution in space group $Pmc2_1$ led to six different two-fold Wyckoff sites (one is occupied by Mo atoms, two by Pt atoms and three by Si atoms).

During the Rietveld refinement, a displacement parameter was refined for each kind of atoms. In agreement with the EPMA results, a small amount (4.7 wt%) of $MoSi_2$ (space group $I4/mmm$, a=3.2042(4), c=7.841(1) Å) was found in the sample. This secondary phase was modelled with scale factor, two cell parameters and one preferred orientation parameter, while the profile parameters were constrained to those of the main phase. $P2_1ma$ being polar, the origin along z was placed on one of the heaviest atom (Pt1) in order to obtain the lowest estimated standard deviations on the coordinates. Finally, 31 parameters were allowed to vary to describe the whole pattern: zero shift, two scale factors, five cell parameters, six profile parameters for the main phase (pseudo-Voigt profile with asymmetry), 11 positional parameters, four atomic displacements and two texture parameters. The background was interpolated between 32 given points. The diffraction pattern is presented in the form of a Rietveld plot in Fig. 1 and the refined structural parameters in Table 3. The value of χ^2 seems to be too high, but it reflects mainly the very high counting statistics of the powder diffraction data obtained for this sample.

3.3. Y phase

The indexation provided by Littner [2] could describe properly most of the peaks present on the pattern of the sample $Mo_{12.5}Pt_{37.5}Si_{50}$ with only slight changes of the lattice parameters. Analysis of the systematic extinctions of Bragg reflections led to the possible space group *Pnma* and $Pn2_1a$. Centrosymmetric group *Pnma* was used for the structure solution, and resulted in the successful determination of 8 four-fold Wyckoff sites (1 is occupied by Mo atom, 3 by Pt atoms and 4 by Si atoms). During the Rietveld refinement a displacement parameter was refined for each kind of atoms. According to the microprobe analysis together with the new phase the sample contains additional phases. Three such phases were found during the detailed phase analysis of the diffraction data: 2.3 wt% of Mo_5Si_3 (structure type W_5Si_3, space group $I4/mcm$), 1.7 wt% of PtSi (structure type FeAs, space group *Pnma*) and 0.9 wt% of Pt_2Si (structure type Fe_2P, space group $P\bar{6}2m$). The presence of these phases is explained by the fact that, at the temperature of annealing, the *Y* phase is in equilibrium with Mo_5Si_3 and the liquid which eventually transforms into PtSi and Pt_2Si after quenching. Due to their small contribution to the diffraction pattern, they were modelled only with scale factors, while the cell parameters were refined first, and fixed in the final cycles of the refinement. In the final refinement cycles, 35 parameters were allowed to vary: zero shift, 4 scale factors, 3 cell parameters, 7 profile parameters for the main phase (pseudo-Voigt profile with asymmetry and anisotropic line broadening of (0k0) reflections), 16 positional parameters, 3 atomic displacements and 1 texture parameter. The background was interpolated between 60 given points. The diffraction pattern is presented in the form of a Rietveld plot in Fig. 2 and the refined structural parameters in Table 4.

Table 3
Atomic coordinates of the *X*–$MoPt_2Si_3$ structure.

Site	Wyckoff position	x	y	z	CN
Mo	2a	0	0.6050(2)	0.000(2)	10
Pt1	2b	1/2	0.0320(1)	0	10
Pt2	2a	0	0.2852(1)	0.0030(9)	10
Si1	2b	1/2	0.2218(9)	0.682(2)	8
Si2	2b	1/2	0.4328(6)	0.168(2)	8
Si3	2a	0	0.1310(8)	0.348(2)	8

Pearson symbol *oP*12, space group $Pmc2_1$, a=3.48438(6), b=9.1511(2), c=5.48253(8) Å.

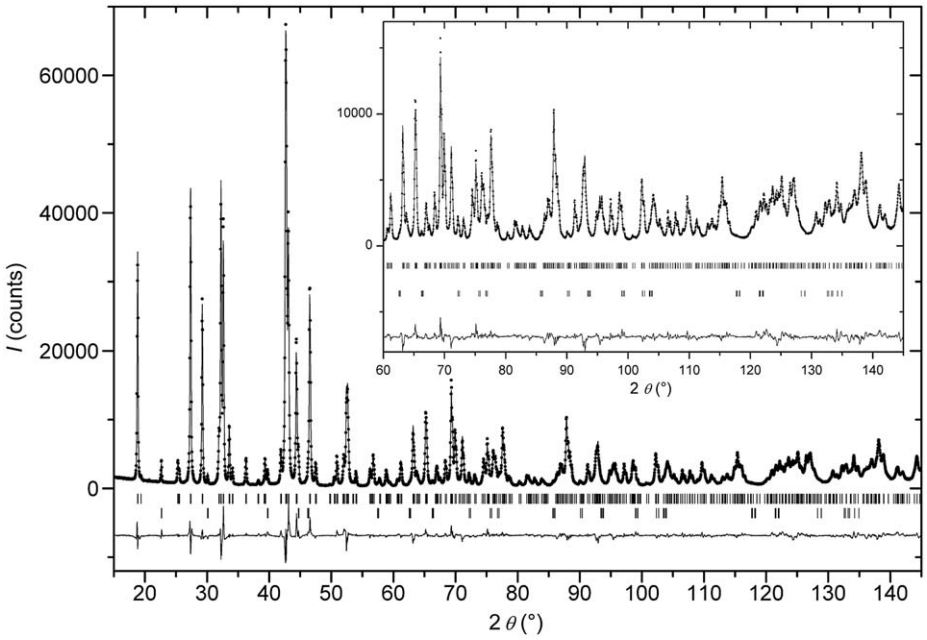

Fig. 1. Rietveld plot of the sample $Mo_{16.7}Pt_{33.3}Si_{50}$. The measured (points) and calculated (line) patterns and difference curve (line below) are shown. The markers indicate the Bragg line positions of the two present phases: *X* and $MoSi_2$ (from top to bottom).

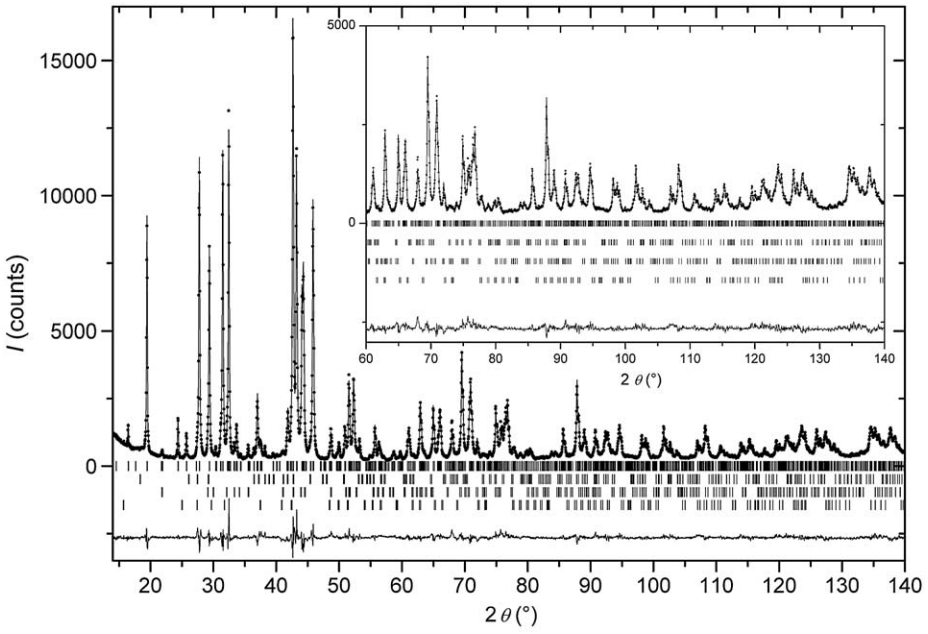

Fig. 2. Rietveld plot of the sample $Mo_{12.5}Pt_{37.5}Si_{50}$. The measured (points) and calculated (line) patterns and difference curve (line below) are shown. The markers indicate the Bragg line positions of the four present phases: *Y* and Mo_5Si_3, PtSi and Pt_2Si (from top to bottom).

Table 4
Atomic coordinates of the *Y*–$MoPt_3Si_4$ structure.

Site	Wyckoff position	*x*	*y*	*z*	CN
Mo	4*c*	0.496(2)	1/4	0.2891(1)	10
Pt1	4*c*	0.003(1)	1/4	0.3306(1)	10
Pt2	4*c*	0.003(1)	1/4	0.5745(1)	10
Pt3	4*c*	0.504(1)	1/4	0.5477(1)	10
Si1	4*c*	0.314(2)	1/4	0.7757(5)	8
Si2	4*c*	0.319(2)	1/4	0.0230(5)	8
Si3	4*c*	0.330(2)	1/4	0.6449(5)	8
Si4	4*c*	0.356(2)	1/4	0.3896(5)	8

Pearson symbol *oP*32, space group *Pnma*, *a*=5.51210(9), *b*=3.49474(7), *c*=24.3090(4) Å.

3.4. Z phase

The indexing of this phase was particularly difficult due to the presence of additional peaks corresponding to secondary phases which had not been evidenced in the EPMA experiment and to the unexpected presence of a slight zero shift in the synchrotron data. The cell was indexed with Topas program, first in a triclinic cell which turned out to be monoclinic. A number of additional lines were found. Most of them could be indexed by Mo_5Si_3 phase (which is in equilibrium with the *Z* phase in the phase diagram). Small other additional lines are present at *d*=2.392 Å (2θ=9.60°), 2.152 Å (2θ=10.67°) and 1.323 Å (2θ=17.40°). These lines could neither be indexed with any of the structures of the phases of the phase diagram nor with any known binary or ternary oxides which could be formed in the system. We considered the possibility that these peaks originate from a superstructure. However, any superstructure able to explain these peaks would be too complex to refine. The most intense peaks were placed in excluded regions during the refinement of the structure.

The analysis of the extinctions revealed that the most symmetric possible space groups could be *C*2/*c* or *Cc*. The mass density was estimated from the density of all the compounds of the ternary Mo–Pt–Si system to be 11.7. The mass of an average atom from the EPMA composition is 106.4 g. The total number of atoms per cell could then be deduced from the cell volume to be approximately 70 atoms (30 Mo, 21 Pt, 20 Si). The structure solution in the space group *C*2/*c* was not successful. Better results were obtained with *Cc*, first without introducing the silicon atoms yielding 8 Mo atoms in general positions (4*a*) and 5 Pt atoms again in general positions. Then Si was introduced and four Si positions in general positions were found giving 68 atoms per cell very close to the 70 estimated atoms.

This trial model was tested with the Rietveld method. After the refinement of the atomic positions of the Mo and Pt atoms, a substantial improvement was brought by the refinement of the occupancy parameters of certain Mo and Pt sites which indicated a higher electron density in the first case and a lower one in the second one. Crystal chemical considerations indicate that the most obvious substitution scheme is Pt substitution on Mo sites and Si substitution on Pt sites.

The space group is polar along *a* and *c* axes. The origin on these two axes was placed on a Pt atom. Pt being the heavy element, lower estimated standard deviations on the coordinates are obtained. The atomic positions of Si are difficult to refine due to the small contribution of this atom to the diffraction compared to Mo and Pt. This results in short atomic distances and, in one case (Si3), in divergence of the refinement. To overcome this problem, we have used restraints for the atomic distances between Si and the neighbouring atoms (Mo–Si: 2.50 Å, Pt–Si: 2.40 Å).

A systematic search for voids in the refined structure was made in order to localize possible missing atoms, for example Si, with no success.

In the final stage of the refinement, 73 parameters were used: zero shift, two scale factors, six cell parameters, five profile parameters (pseudo-Voigt profile, different for the two phases), 49 positional parameters, seven occupancy parameters, three atomic displacements. The background was interpolated between 40 selected points. The diffraction pattern is presented in the form of a Rietveld plot in Fig. 3 and the refined structural parameters in Table 5.

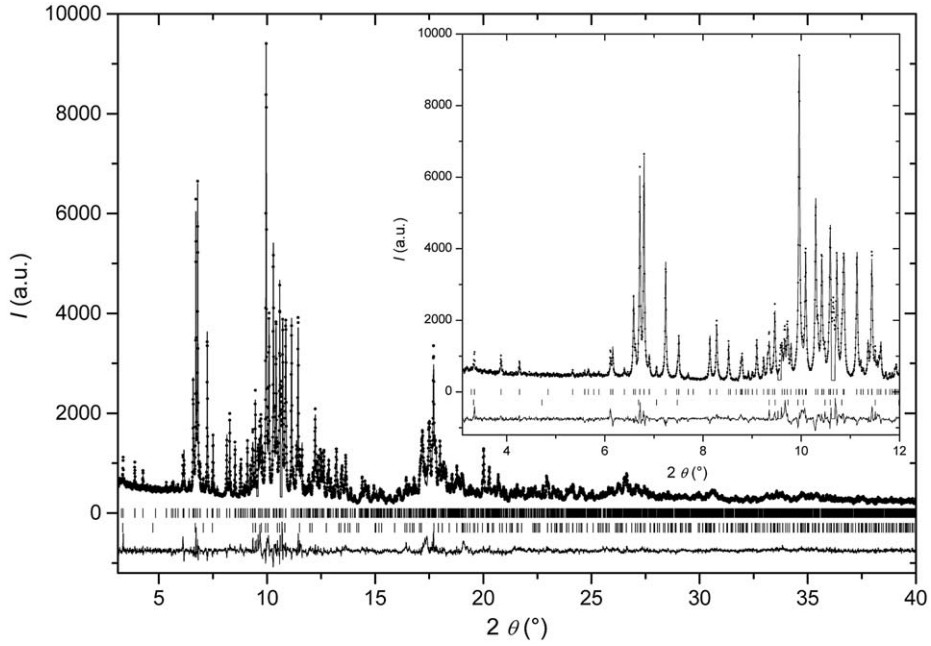

Fig. 3. Rietveld plot of the sample $Mo_{42.9}Pt_{28.6}Si_{28.6}$. The measured (points) and calculated (line) patterns and difference curve (line below) are shown. The markers indicate the Bragg line positions of the two present phases: *Z* and Mo_5Si_3 (from top to bottom). The inset shows a zoom of the first part of the diagram and, in particular, the two excluded regions.

Table 5
Atomic coordinates and occupancy parameters of the *Z* phase structure.

Site	Atom	Wyckoff position	*x*	*y*	*z*	Occupation (atom/site)	CN
Mo1	Mo	4*c*	0.0100(5)	0.597(1)	0.2753(8)	4	13
Mo2	Mo	4*c*	0.6848(6)	0.2911(9)	0.4117(9)	4	13
Mo3	Mo	4*c*	0.1670(7)	0.067(1)	0.194(1)	4	14
Mo4	Mo	4*c*	0.6789(5)	0.1981(8)	0.1641(8)	3.24(6)	13
	Pt					0.76(6)	
Mo5	Mo	4*c*	0.3382(6)	0.0778(8)	0.7809(8)	2.97(7)	13
	Pt					1.03(7)	
Mo6	Mo	4*c*	0.6800(6)	0.928(1)	0.3771(8)	4	15
Mo7	Mo	4*c*	0.4974(6)	0.584(1)	0.6918(9)	4	14
Mo8	Mo	4*c*	0.8501(6)	0.097(1)	0.3804(8)	3.73(6)	15
	Pt					0.27(6)	
Pt1	Pt	4*c*	0	0.6493(5)	0	4	10
Pt2	Pt	4*c*	0.0051(4)	0.2526(7)	0.2455(7)	3.79(4)	10
	Si					0.21(4)	
Pt3	Pt	4*c*	0.7724(3)	0.8953(5)	0.1375(5)	3.88(3)	12
	Si					0.12(3)	
Pt4	Pt	4*c*	0.4921(3)	0.6541(5)	0.9743(5)	3.76(4)	10
	Si					0.24(4)	
Pt5	Pt	4*c*	0.2521(4)	0.1049(4)	0.4831(7)	3.52(3)	10
	Si					0.48(3)	
Si1	Si	4*c*	0.085(1)	0.395(1)	0.064(3)	4	11
Si2	Si	4*c*	0.8581(7)	0.855(3)	0.602(2)	4	11
Si3	Si	4*c*	0.8467(4)	0.6331(9)	0.0878(8)	4	11
Si4	Si	4*c*	0.371(2)	0.229(3)	0.366(3)	4	11

Pearson symbol *mC*68, space group *Cc*, $a=13.8868(3)$, $b=8.0769(2)$, $c=9.6110(2)$ Å, $\beta=100.898(1)^\circ$; $B_{Mo}=0.90(4)$, $B_{Pt}=0.33(1)$, $B_{Si}=0.7(3)$ Å^2, refined composition $Mo_{29.9(2)}Pt_{21.0(3)}Si_{17.1(1)}$.

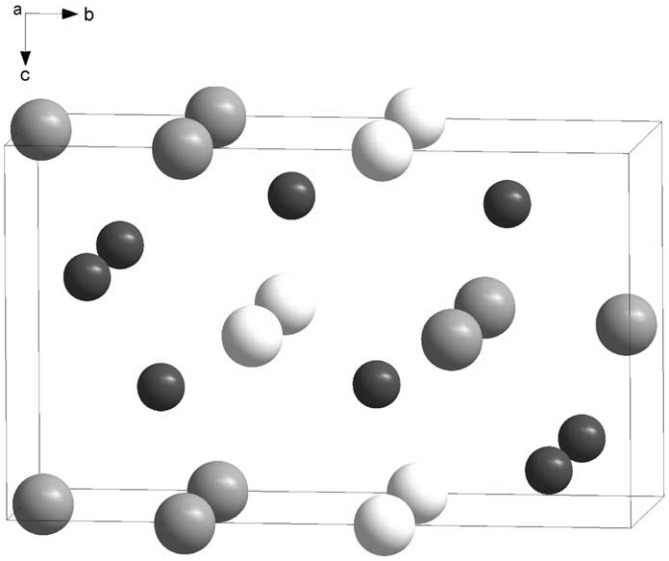

Fig. 4. Unit cell content of *X*–$MoPt_2Si_3$ phase (Mo in white, Pt in grey, Si in black).

4. Discussion

4.1. X and Y phases

Both structures represent new structure types, and both derive from the structure of the binary PtSi compound (structure type FeAs, space group *Pnma*, Pearson code *oP*8, $a=5.577$ Å, $b=3.587$ Å, $c=5.916$ Å [9]). *X* ($MoPt_2Si_3$) and *Y* ($MoPt_3Si_4$) contain the same amount of silicon (50 at%) as PtSi, and derive from this structure by ordered replacement of Pt by Mo in different amount, followed by displacements. In the *Y* phase, the replacement of one fourth of the Pt atoms leads to an increase of one cell parameter ($c_X=4c_{PtSi}$). Further replacement of Pt by Mo atoms in the *X* phase (one third) leads to the stabilization of a new ordered non-centrosymmetric structure with ordering along the same direction ($b_Y=3/2c_{PtSi}$). The unit cells of the two structures are shown in Figs. 4 and 5. The coordination numbers for each atom within the coordination sphere of 3.1 Å (see Tables 3 and 4) are identical to those in PtSi and the observed polyhedra are very similar. In both structures the coordination polyhedra derive from the polyhedra typical for close-packed structures. Around *d*-metal atoms anticubooctahedra with two additional atoms are formed (defect for Pt atoms). The closest atomic environments of the Si atoms also form polyhedra,

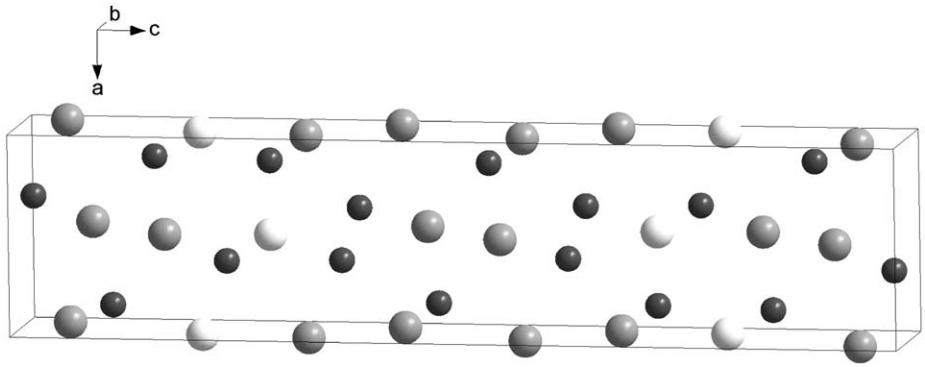

Fig. 5. Unit cell content of *Y*–$MoPt_3Si_4$ phase (Mo in white, Pt in grey, Si in black).

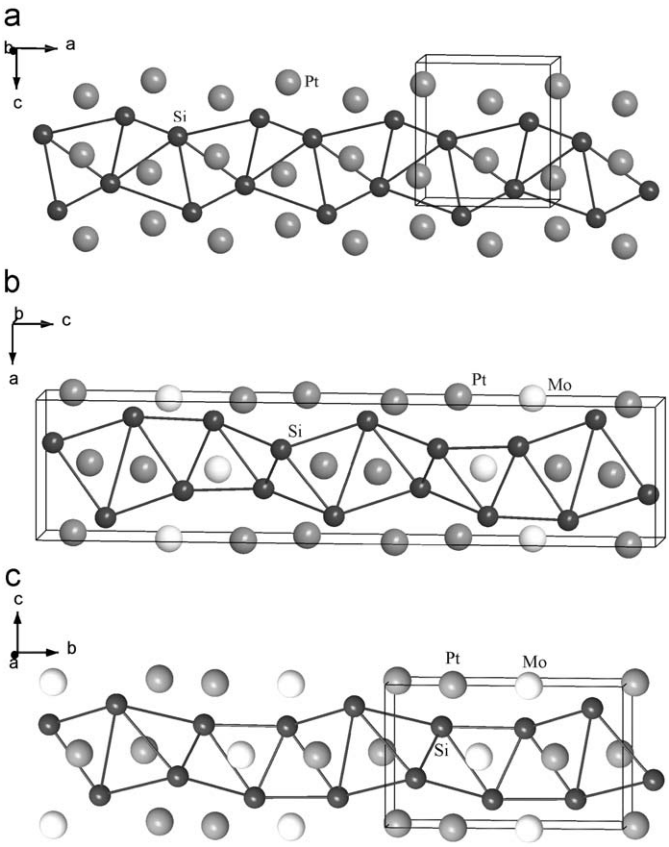

Fig. 6. Corrugated ribbons from Si atoms in the structure of PtSi (a), *Y* (b) and *X* (c) (Mo in white, Pt in grey, Si in black).

derivative from cubooctahera or anticubooctahedra with some additional or missing atoms (Fig. 7).

In both ternary structures *Y* and *X*, silicon atoms form infinite corrugated ribbons along long lattice parameters (*b* in *X* and *c* in *Y*). These ribbons remain almost unchanged compared to the structure of PtSi binary compound (see Fig. 6).

All three structures are constructed from the same "building blocks" and obviously are the members of the same structural family. However, ordered substitution of Pt atoms by Mo atoms in the structure of PtSi leads to the shift of the *d*-atoms from the "ideal" positions, influencing also Si-atoms ribbons, leading to the deformation of the unit cell, which results in two new ternary structure types. Such behaviour cannot be explained by atomic size effect ($r_{Mo}=r_{Pt}=1.39$ Å), but can be explained by stronger interaction between Pt and Si atoms than between Mo and Si (the shortest Pt–Si interatomic distances are 2.388 Å (in *X*) and 2.355 Å (in *Y*), whereas Mo–Si are 2.518 Å (in *X*) and 2.463 Å (in *Y*)).

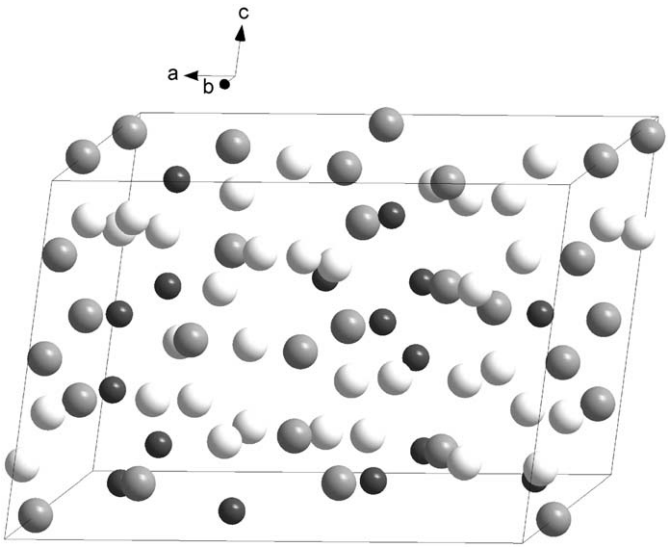

Fig. 7. Unit cell content of *Z*–$Mo_{32}Pt_{20}Si_{16}$ (Mo in white, Pt in grey, Si in black).

4.2. Z phase

This third structure represents also a new structure type (see Fig. 7). The analysis of the coordination polyhedra of the *Z* phase reveals an arrangement quite different from what is observed for *X* and *Y* phases. Mo atoms have CN from 13 to 15, Pt atoms from 10 to 12 and Si atoms are always coordinated by 11 atoms (see Table 5). All the coordination polyhedra possess a large amount of triangular faces and are or resemble Frank-Kasper polyhedra. In particular, the silicon polyhedra are very close to icosahedra with a missing atom. This type of coordination is very common for Si in intermetallic compounds like e.g. $Hf_2Ni_3Si_4$, $Hf_2Ru_3Si_4$ and Mn_5Si_3 structure types (in our system Mo_5Si_3 crystallizes in this latter structure type). The tendency for Mo (*bcc* element, *d* electron-poor) to occupy the higher CN sites and Pt (*fcc* element, *d* electron-rich) the lower CN sites is also typical for Frank-Kasper phases in which the site preference results more from the position in the periodic table than from the atomic sizes (Mo and Pt have the same metallic radius).

The shortest calculated distances involve always Si atoms. For example, the distance between Pt and Si can be as short as 2.35 Å, which is much shorter than the sum of metallic radii but which

compares very well with distances found in many silicides, including in Pt–Si systems ($Pt_{12}Si_5$: 2.24 Å [10], PtSi: 2.41 Å [9]).

The presence of a Frank-Kasper, or Frank-Kasper related phase in this system is not very surprising, in particular in the Si-poor region of the phase diagram. The *A*15 Frank-Kasper phase is stable in both Mo–Si and Mo–Pt binary systems with a continuous ternary extension between the two phases [3,4]. In a very similar system (Mo–Ru–Si) both σ and χ Frank-Kasper phases have been evidenced close to the Mo–Ru binary system [11].

One may notice non-negligible discrepancies between refined ($Mo_{44.0}Pt_{30.9}Si_{25.1}$) and measured ($Mo_{42.5}Pt_{29.6}Si_{27.9}$) phase composition. The refinement of site occupancies has led to an improvement compared to the stoichiometric (completely ordered) composition ($Mo_{32}Pt_{20}Si_{16}$=$Mo_{47.1}Pt_{29.4}Si_{23.5}$) with a simple model of substitution of Mo by Pt and of Pt by Si. However, one can not exclude that the substitution scheme is more complex and that the three elements may occupy the same sites with different occupancy parameters. This is typical for Frank-Kasper phases (see e.g. the determination of the site occupancies in the μ phase in Zr–Nb–Al system [12] and in the σ and χ phases in Mo–Ru–Si system [11]. This problem cannot be solved from a single data set. Joint refinement of multiple-wavelength resonant diffraction data would be necessary to perform an accurate refinement of the ternary site occupancies and obtain a better agreement between refined and measured compositions.

5. Conclusion

In the Mo–Pt–Si system, three ternary intermetallic compounds have been evidenced. The three compounds possess original crystal structures that have been determined *ab initio* from powder diffraction data in the present work. The crystal structure of the two phases *X* and *Y* derive from the PtSi structure. On the contrary, the crystal structure of the *Z* phase is related to Frank-Kasper phases, in agreement with the lower silicon content.

Acknowledgments

The authors wish to acknowledge Amir Farzadfar for the synthesis of the *Y* phase, the European Synchrotron Radiation Facility and the Swiss Norwegian Beamline for providing us beamtime and Herman Emerich, our local contact. Financial support from the Agence Nationale de la Recherche (grant ANR-06-Blan-0181, Mitect project) is acknowledged.

Appendix A. Supplementary material

Supplementary data associated with this article can be found in the online version at doi:10.1016/j.jssc.2009.11.006.

References

[1] A.K. Vasudévana, J.J. Petrovicb, Mater. Sci. Eng. A 155 (1–2) (1992) 1–17.
[2] A. Littner, Thèse de Doctorat, Université de Nancy Henri-Poincaré, 2003.
[3] T. Benlaharche, Thèse de Doctorat, Université de Nancy Henri-Poincaré, 2008.
[4] J.-M. Fiorani, N. David, M. Vilasi, J. Phase Equilibr., 2009, to be published.
[5] A. Boultif, D. Louër, J. Appl. Crystallogr. 24 (1991) 987–993.
[6] TOPAS, version 3. 1999: Bruker AXS.
[7] V. Favre-Nicolin, R. Černý, J. Appl. Crystallogr. 35 (2002) 734–743.
[8] J. Rodríguez-Carvajal, Newsletter (26) (2001) 12–19.
[9] E.J. Graeber, R.J. Baughman, B. Morosin, Acta Crystallogr. B 29 (1973) 1991–1994.
[10] W. Gold, K. Schubert, Z. Kristallogr. 128 (1969) 406–413.
[11] J. Tobola, M. François, E. Elkaim, J.-M. Joubert, M. Vilasi, Intermetallics (2009), in press.
[12] J.-M. Joubert, R. Černý, H. Emerich, Z. Kristallogr. Suppl. 26 (2007) 311–316.